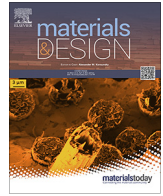




Contents lists available at ScienceDirect

Materials & Design

journal homepage: www.elsevier.com/locate/matdes

Surface treatment of 3D printed Cu-bearing Ti alloy scaffolds for application in tissue engineering

Zhe Yi^{a,1}, Ying Liu^{a,b,1}, Yidan Ma^a, Zhaogang Liu^{a,b}, Hui Sun^a, Xing Zhou^d, Rui Kang^{a,c}, V.A.M. Cristino^e, Qiang Wang^{a,*}

^aSchool and Hospital of Stomatology, China Medical University, Liaoning Provincial Key Laboratory of Oral Diseases, Shenyang 110002, China

^bDepartment of Stomatology, Taian City Central Hospital, Taian 271000, China

^cSchool of Stomatology, Jiamusi University, Jiamusi 154004, China

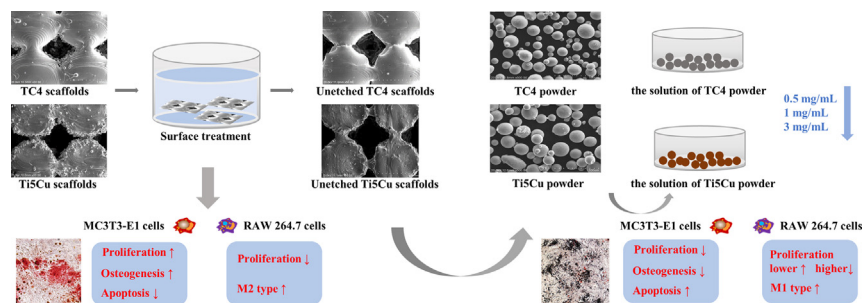
^dShenyang National Laboratory for Materials Science, Northeastern University, Shenyang 110819, China

^eDepartment of Electromechanical Engineering, University of Macau, Avenida da Universidade, Taipa, Macao, China

HIGHLIGHTS

- Surface treatment can enhance the biocompatibility of the 3D printed Ti scaffolds.
- Etched Ti5Cu scaffolds showed higher proliferation, lowest apoptosis rate and the best early osteogenic ability.
- Higher concentration powders inhibited the proliferation and osteogenic differentiation of MC3T3-E1 cells, as well as promoted apoptosis.

GRAPHICAL ABSTRACT



ARTICLE INFO

Article history:

Received 5 July 2021

Revised 1 November 2021

Accepted 21 December 2021

Available online 23 December 2021

Keywords:

Surface treatment

3D printing

Ti scaffolds

MC3T3-E1 cells

RAW 264.7 cells

ABSTRACT

3D printed medical titanium alloy has shown great advantages in manufacturing complex and personalized scaffolds for tissue engineering. To promote the repair of bone defects, fabrication of a scaffold with high accuracy and excellent cell behaviors is required. However, the partially melted or un-melted powders must be removed in the post-process. In this study, the effects of unfused metal powders on the biocompatibility of 3D printed Ti alloy scaffolds were analyzed by co-culture with MC3T3-E1 cells and RAW 264.7 cells, and the surface treatment strategy was proposed. Results showed that surface treatment can enhance the biocompatibility of the 3D printed Ti alloy scaffolds. The vitro tests with MC3T3-E1 cells demonstrated that the ETi5Cu (etched Ti5Cu) showed the better cell proliferation and osteogenic potential, and the lower cell apoptosis rates. Moreover, higher concentration of powders showed inhibitory effects on cytocompatibility and osteogenesis of MC3T3-E1 cells, and promoted the polarization of macrophages to M1 type. In summary, the removal of metal powders on the 3D printed scaffolds plays an important role in the biological performance, which provided a promising strategy for the application of Ti implants.

© 2021 The Authors. Published by Elsevier Ltd. This is an open access article under the CC BY-NC-ND license (<http://creativecommons.org/licenses/by-nc-nd/4.0/>).

* Corresponding author at: School and Hospital of Stomatology, China Medical University, Liaoning Provincial Key Laboratory of Oral Diseases, No. 117 Nanjing North Street, Shenyang 110002, China.

E-mail address: mfgwang@cmu.edu.cn (Q. Wang).

¹ Co-first authors contributed equally.

1. Introduction

Titanium implants are widely used in dentistry and orthodontic fixation due to their good mechanical performance and its biocompatibility. Currently, multiple techniques are available for the manufacture of titanium implants [1,2]. Indeed, porous metal-

lic biomaterials have become an interesting approach to improve long-term fixation of Ti devices. The development of bioactive Ti scaffolds for bone regeneration remains a challenge which needs the design of Ti implants with enhanced osseointegration. 3D printing technology is able to process complex or personalized scaffolds to better match the bone tissue, which stands for one of the development direction of new metal medical devices [3,4]. Previous researches have proved that porous structures were beneficial to osteoblastic adhesion, proliferation and differentiation [5]. Porous materials bone implants have network pores that allow cells to grow in and ensure proper vascularization [6]. It was reported that the pore size affects the adhesion and proliferation of osteoblasts. When the pore diameter is greater than 200 μm , the size is the most suitable for osteosynthesis and angiogenesis, and an excessively small pore size will affect the proliferation of osteoblasts and angiogenesis [7,8]. However, larger pore size may lead to negative effects of cell-to-cell connection and osteogenesis [9,10]. Moreover, the pore shape has a significant effect on the biological properties of scaffolds [11]. Experiments have shown that rhomboid holes can promote bone insertion more than round ones, and the rhomboid holes have better mechanical properties due to their supporting role [3,12].

However, 3D printing technology uses metal powder as the raw material, which often results in incomplete melting of the powder or attachment of the powder on the product structure [13-17]. Hence, there may be residual powders attached on the Ti scaffolds in the manufacturing process. When these Ti alloys were implanted, the powders released by the metal implant inevitably deposited into the surrounding tissue, leading to aseptic loosening of the implant or osteolysis around the prosthesis, which, over time, can lead to heart, kidney disease and even cancer in humans [18-24].

Various studies have shown that the behavior of osteoblasts was affected by powder size [25]. When the powder size is smaller than 10 μm , the metal powder will enter the osteoblast, and affect the release of osteoblast factor resulting in osteolysis [26]. If the metal powder is within the range of 10 ~ 100 μm , the cell proliferation can be affected by the interaction between powders and cells [27], and if the diameter of Ti alloy powder was higher than 100 μm , the growth of osteoblasts can be seriously hindered [28]. Other studies have reported that the accumulation of Ti alloy powder in the body would lead to the toxicity and can seriously harm the health of the individual [23]. Ti powders exhibited toxicity to cells at all used concentrations (0.1–1 mg/mL), while the range from 0.6 to 1 mg/mL to can cause enough damage [23]. In the study on the effects of different concentrations of Ti particles on osteoblasts, the concentration of Ti powders ranging from 0.1 to 0.5 mg/mL was low concentration, and ranging from 0.6 to 1 mg/mL was high concentration [23].

The shedding of these residual powders not only inhibit bone formation, but also stimulates inflammation [29-31]. Macrophages play a major role in the immune response affecting implants, such as regulating bone remodeling, tissue repair, and tissue response to biomaterials [32]. Macrophages have high plasticity after activation and can differentiate into classically activated (M1 phenotype) and alternatively activated (M2 phenotype) depending on environment stimuli [33]. After the Ti alloys are implanted into the bone, the shed Ti alloy powders had an immune reaction with macrophages [34]. At the early stage of inflammation, macrophages polarize into M1 type, mainly secreting pro-inflammatory factors and chemokines. With the repair of tissue damage, macrophages are activated as type M2, and the increase of M2 type macrophages can enhance the release of osteogenic factors, secrete anti-inflammatory factors, reduce inflammatory response, and promote new bone formation as well as tissue healing [35]. Copper (Cu) is known to be an essential trace element in the human body [36]. It not only participates in cell function and protein synthesis but

also promotes angiogenesis and proliferation and differentiation of osteoblasts [37-39]. Furthermore, Cu plays an important role in physiological repair processes such as wound healing and new bone formation [40,41]. In addition, several studies have proved that copper can inhibit the expression of pro-inflammatory cytokines and increase the secretion of anti-inflammatory cytokines in macrophages [28,42].

In our previous study, a series of Ti-xCu alloys with different Cu contents (3, 5 and 7 wt%) were fabricated and systematically studied. The results demonstrated that Ti-5Cu alloy exhibited extremely strong antibacterial properties, good biological compatibility and osteogenic ability, as well as the most excellent ductility and corrosion resistance [43]. Based on previous studies, Ti5Cu scaffolds were used in the present study. This study emphasizes on the potential impact of the unfused metal powders should be seriously considered when 3D printed Ti alloy scaffolds are used as implants. The biological behaviors of MC3T3-E1 cells and RAW 264.7 cells were evaluated by co-culture with Ti alloy scaffolds before and after removing attached powders. The biological responses of MC3T3-E1 cells and RAW 264.7 cells to different concentrations of metal powders were also assessed to further demonstrate the effect of the residual powders on 3D printed Ti alloy scaffolds. This study aims to provide a theoretical basis for better and more systematic assessment of the biological response of 3D printed metal implants containing residual powders for potential orthopedic application.

2. Materials and methods

2.1. Material preparation

Scaffold samples with a size of 10 × 10 × 2 mm was prepared by 3D printing technology using mixture powders consisting of Cu and Ti. 3D Systems (ProX DMP 200, US) were processed with a laser beam with a wavelength of 1070 nm using TC4 and Ti5Cu powders (Avimetal powder metallurgy technology Co., Ltd, China) with a diameter ranging from 20 to 40 μm . Our previous study compared different laser processing parameters and selected the optimal parameters in this study: laser power of 260 W, laser spot size of 70 μm , scanning distance of 45 μm , and the layer thickness of 45 μm [44]. The specimens were subsequently immersed in diluted hydrofluoric acid solution with a concentration of 40% in an ultrasonic bath for 1 min to remove the un-melted metal powders. Fig. 1 illustrates the flow diagram of the present study.

All samples were divided into four groups: unetched Ti6Al4V (TC4), unetched Ti5Cu (Ti5Cu), etched Ti6Al4V (ETC4), etched Ti5Cu (ETi5Cu). The specimens were ultrasonically etched with acetone, ethyl alcohol, distilled water for 10 min and then sterilized at 121 °C for 20 min.

2.2. Surface characterization

2.2.1. Microstructure and phase composition

The structural morphologies of Ti alloy scaffolds were characterized by an optical microscope (KMM-800, Shanghai SiChangYue, China) and scanning electron microscope (SEM, Zeiss, Germany) equipped with EDS. The phase composition of the coatings was analyzed by an X-ray diffractometer (XRD, Philips PW1700) at a scanning speed of 5°/min ranging from 10° to 80° with using CuK α radiation.

2.2.2. Roughness measurement

The average three-dimensional roughness (Sa) of unetched and etched samples was detected by the white-light interferometer

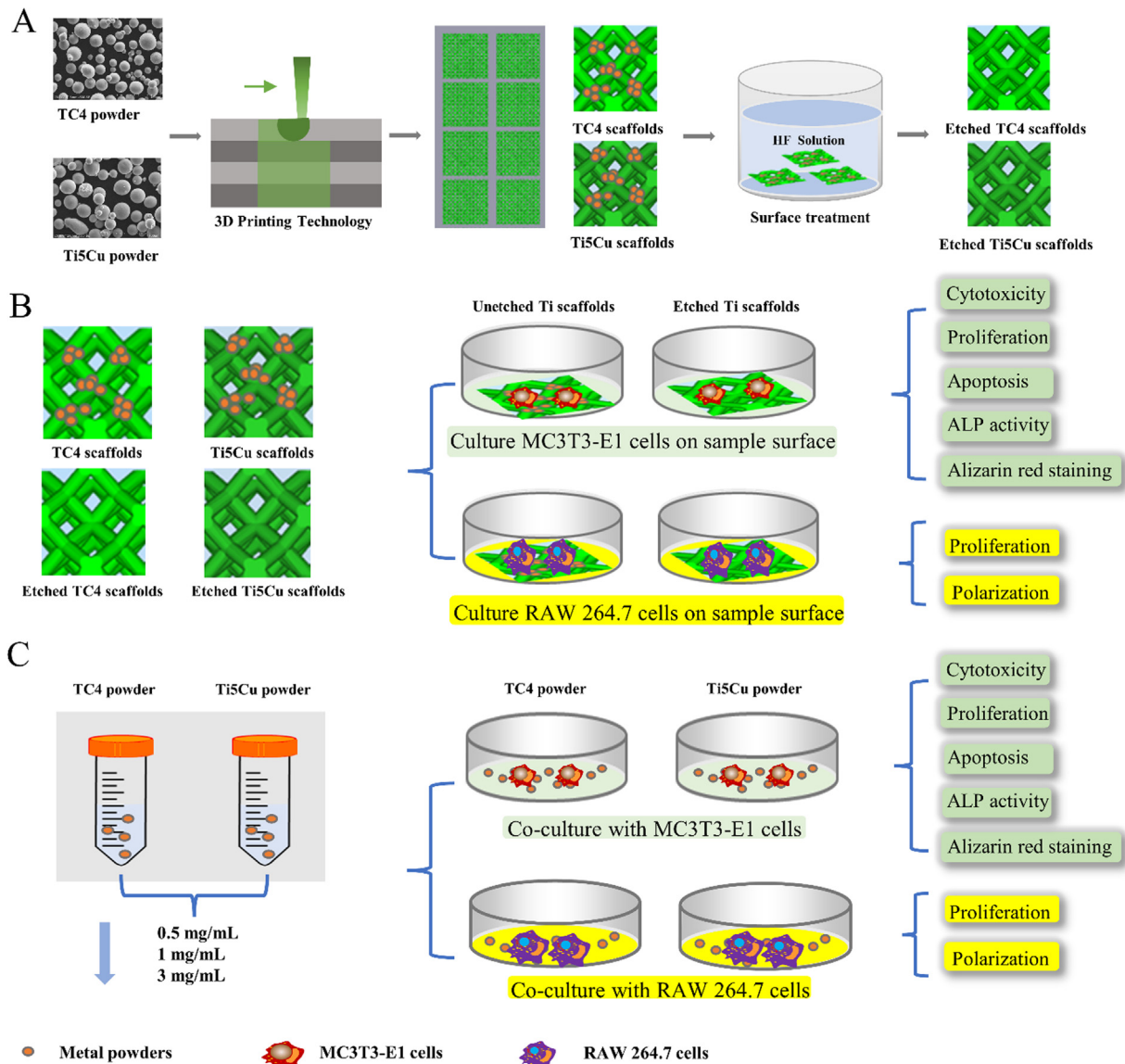


Fig. 1. Flow diagram of the study: (A) Preparation of Ti alloy scaffolds; (B) Behaviors of MC3T3-E1 cells and RAW 264.7 cells on Ti alloy scaffolds before and after surface treatment; (C) The biological responses of MC3T3-E1 cells and RAW 264.7 cells to metal powders.

(Phase shift MicroXAM-3D, ADE, USA). Three samples were taken for each group and three randomly selected areas per sample.

2.3. Cell culture

2.3.1. MC3T3-E1 cells

The MC3T3-E1 cells were cultured in alpha minimum essential medium (α -MEM) supplemented with 10% (v/v) fetal bovine serum (FBS) and 1% penicillin and streptomycin in a humidified atmosphere at 37 °C with 5% CO₂. When the monolayer reached sub-confluence, the cells were sub-cultured by 0.25% trypsinization. The third or fourth generations were used in subsequent experiments. MC3T3-E1 cells were used in the tests of cell proliferation, cytotoxicity, early osteogenic and apoptosis.

2.3.2. RAW 264.7 cells

RAW 264.7 cells were cultured in Dulbecco's modified Eagle's medium (DMEM) supplemented with 10% (v/v) heat-inactivated fetal bovine serum and 1% penicillin and streptomycin. The culture was maintained in an incubator with 5% CO₂ at 37 °C. RAW 264.7 cells were used to the test of cell proliferation and polarization.

2.4. Cells cultured on Ti alloy scaffolds

2.4.1. Cell proliferation and cytotoxicity test

The CCK-8 assay (US Everbright Inc., Silicon Valley, USA) was performed to evaluate the viability of MC3T3-E1 cells. The cells were cultured at a concentration of 1×10^4 cells/mL and then seeded on all samples in a 12-well culture plate (Corning, China) in a humidified atmosphere with 5% CO₂ at 37 °C. After incubated for 1 d, 3 d, 5 d and 7 d, respectively, the culture media was removed and these samples were rinsed with phosphate buffered saline (PBS) twice. A 10% (v/v) concentration of CCK-8 reagent was added and the samples were incubated in a dark incubator for 2 h at 37 °C. Afterwards, 100 μ L of medium from each well was moved to a 96-well culture plates, and the 450 nm optical density (OD) was used with an Enzyme standard instrument (Tecan, Austria). The cell relative growth rate (RGR) was calculated according to Eq. (1):

$$\text{RGR}(\%) = \text{OD}_{\text{experimentalgroup}} / \text{OD}_{\text{controlgroup}} \times 100\% \quad (1)$$

2.4.2. Cell apoptosis assay

The cell apoptosis was quantified by FCM analysis using Annexin V-FITC/PI apoptosis detection kit (US Everbright Inc., Silicon Valley, USA) according to the manufacture’s protocol. MC3T3-E1 cells were seeded onto the different sample surfaces at a density of 1×10^5 cells/well in 12-well plates. After incubated for 3 d and 7 d, the cells were washed two times with pre-cooled PBS, digested

with 0.25% trypsin (without EDTA) and transferred into EP tubes. The cells were then washed in ice-cold PBS, re-suspended in 100 μ L binding buffer and incubated with 5 μ L Annexin V-FITC and 5 μ L propidium iodide (PI) for 15 min at 4 $^{\circ}$ C in the dark. Finally, 400 μ L of binding buffer was added to each tube, the cells apoptosis was analyzed with flow cytometer (BD, LSRFortessa, USA).

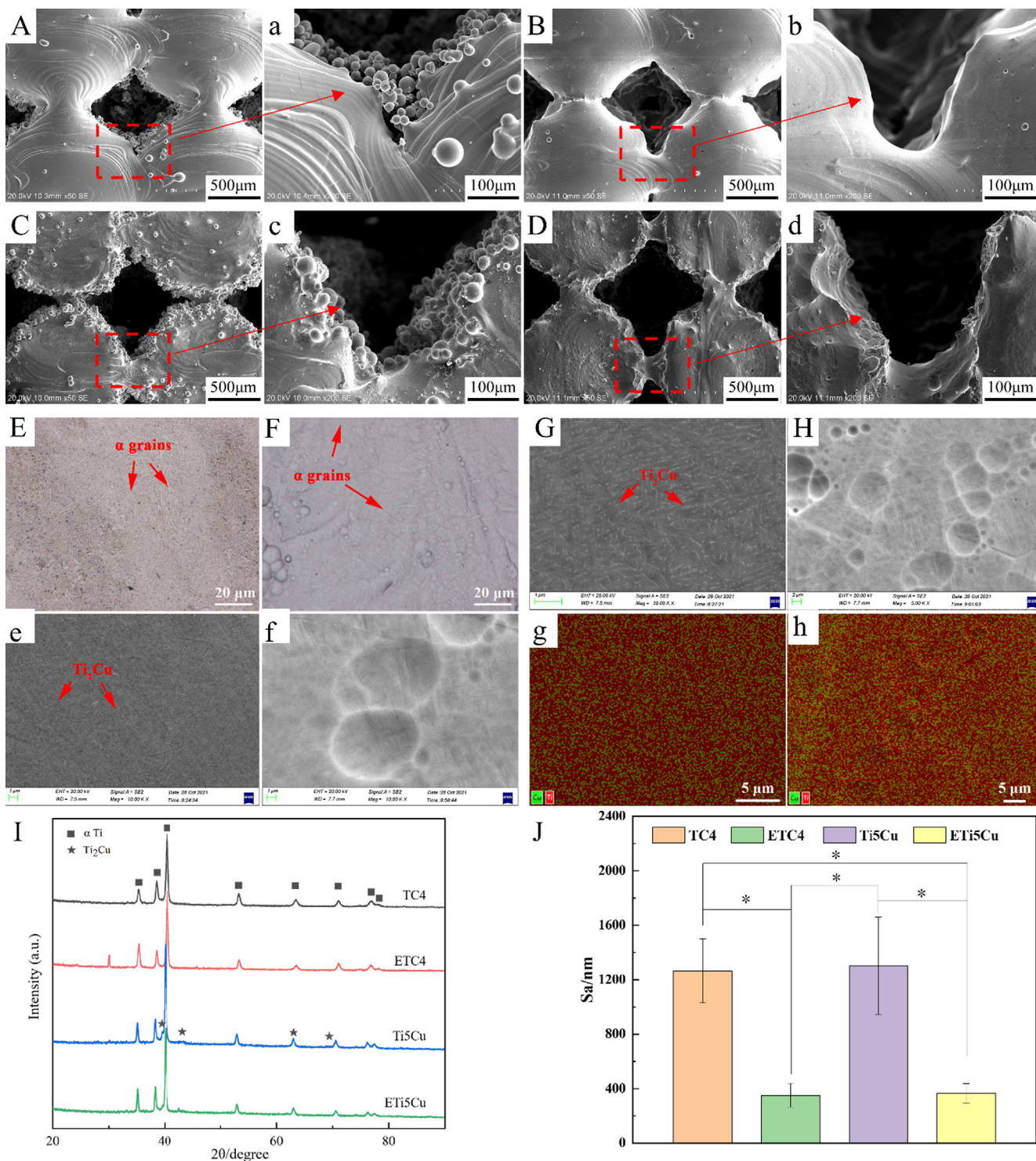


Fig. 2. SEM images of Ti alloy scaffolds (A-d): (A, a) TC4; (B, b) ETC4; (C, c) Ti5Cu; (D, d) ETi5Cu. The morphology of Ti5Cu samples before and after etching under optical microscope (E, F) and the morphology under SEM (e, f): (E, e) Ti5Cu; (F, f) ETi5Cu. SEM images (G, H) and the corresponding EDS results (g, h) of Ti5Cu samples before and after etching: (G, g) Ti5Cu; (H, h) ETi5Cu. XRD patterns of TC4 and Ti5Cu samples before and after etching (I). The surface roughness of Ti alloy scaffolds (J).

2.4.3. ALP activity

MC3T3-E1 cells were seeded onto different sample surfaces at a density of 1×10^5 cells/well into 12-well plates. After 24 h culture, the culture medium was replaced with an osteogenesis-inducing solution, which was changed every 2 d. After 7 and 14 days of culture, the activity of alkaline phosphatase (ALP) was analyzed with Alkaline Phosphatase Assay Kit according to the manufacturer's instructions (Beyotime, China), and the total protein concentration was measured by a BCA protein assay kit (Beyotime, China). The ALP activity of each sample was normalized as ALP/total protein.

2.4.4. Alizarin red staining

MC3T3-E1 cells were seeded onto different sample surfaces at a density of 1×10^5 cells/well into 12-well plates. After 24 h culture, the culture medium was replaced with an osteogenesis-inducing solution, which was changed every 2 d. After 28 and 35 days of culture, cells were washed, fixed and then incubated with Alizarin Red S Staining Kit for Osteogenesis according to the manufacturer's instructions (Beyotime, China). Finally, the amount of Alizarin red bound to the calcium nodules was quantified by dissolving the stained sample into 1% cetylpyridinium chloride (CPC) solution and reading the optical density at 562 nm using microplate reader (Infinite M200, Tecan, Austria).

2.4.5. Macrophage proliferation

RAW 264.7 cells were seeded onto the surface of all samples at a concentration of 1×10^5 cells in 12-well plates. After incubated for 24 h, 48 h and 72 h, respectively, the culture media was removed and the samples were etched with PBS two times. The cells were then incubated with CCK8 solution for 2 h and the optical density

was measured by microplate reader (Infinite M200, Tecan, Austria) at 450 nm.

2.4.6. Macrophage polarization

The polarization state of macrophages in response to the implant microenvironment was determined by flow cytometric analysis. RAW 264.7 cells were seeded onto the surface of all samples at a concentration of 1×10^5 cells/well. After cultured for 24 h, cells were washed and then incubated for 30 min with APC-conjugated CD86 (Thermo Fisher Scientific, 17-0862-81) and PE-conjugated CD206 (Thermo Fisher Scientific, 12-2061-80). Finally, the results were acquired using a flow cytometer (Becton Dickinson, America).

2.5. Cell responses to metal powders

2.5.1. Preparation of metal powders

The metal powders in this study were the starting material from which the scaffolds are manufactured. The real powder concentration on the surface of unetched samples was determined by calculating the weight loss before and after etching. The calculation formula was Eq. (2):

$$C = (W_1 - W_2 - \Delta W) / V \tag{2}$$

where C (mg/mL) is the concentration of metal powders, W_1 (mg) is the weight of the unetched scaffold sample, W_2 (mg) is the weight of the etched scaffold sample, ΔW (mg) is the weight loss of the etched scaffold sample before and after etching within the same time, V (mL) is the volume of the immersion solution. The highest concentration value of the powder was 3 mg/mL by

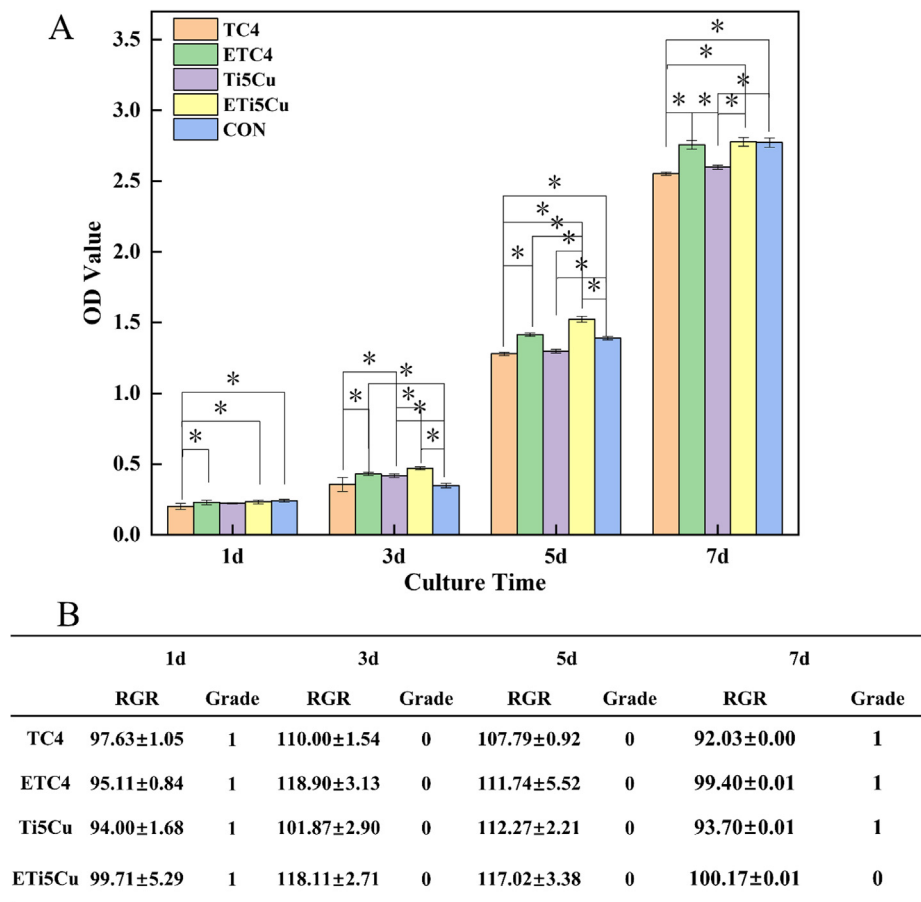


Fig. 3. (A) Optical density of MC3T3-E1 cells measured by CCK8 test and (B) relative growth rate (RGR) and cytotoxicity level at different detection period (n = 5, * p < 0.05).

calculating the weight loss before and after etching. Based on above, TC4 powders and Ti5Cu powders (named PTC4 and PTi5Cu) with three concentrations of 0.5 mg/mL, 1 mg/mL and 3 mg/mL were selected to further demonstrate the effect of the residual powders on the biological properties of scaffold samples. The powders were initially submerged for 48 h in 70% ethanol and dried in an aseptic incubator. Then the solution of metal powders was prepared by adding the required amount of metal powders into the cell culture media.

2.5.2. The effect of metal powders on the cells

The cytotoxic effects and proliferation ability of metal powders to MC3T3-E1 cells were evaluated using the CCK8 assay on 1 d, 3 d, 5 d and 7 d. To determine the apoptosis rates of MC3T3-E1 cells cultured with metal powders, flow cytometry was performed followed by Annexin V-FITC/PI double staining after cultured for 3 d and 7 d. The effect of metal powders on the early osteogenic differentiation of MC3T3-E1 cells was determined with ALP assay after cultured for 7 d and 14 d. Staining with Alizarin Red S was performed in order to observe calcium deposition after cultured for 28 d and 35 d.

Macrophage activity co-cultured with metal powders was analyzed using CCK-8 assay on 24 h, 48 h and 72 h. The polarization state of macrophages in response to metal powders was determined by flow cytometric analysis on 24 h.

2.6. Statistical analysis

All experiments were repeated at least three times for statistical purpose. Statistical analysis was performed with SPSS 25.0 software. Differences between groups were analyzed using one-way analysis of variance (ANOVA) followed by Tukey's test.

3. Results

3.1. The characterization of Ti alloy scaffolds

Fig. 2 shows the microstructures of TC4 scaffolds and Ti5Cu scaffolds before and after etching. SEM analysis revealed that the pore size of the scaffold was relatively uniform, with a rhomboid porous structure. The scaffolds showed a three-dimensional structure with the pore size of about 500 μm . A large number of Ti alloy

powders were distributed on the surface of the Ti alloy scaffolds, and the powder is more distributed in the connection parts of the pores. It can be observed in Fig. 2C and D that the surface of the etched Ti alloy scaffolds was smooth and the un-melted powders were absent on the etched Ti alloy scaffolds, indicating that the surface treatment was successful for removing the un-melted powders.

Fig. 2E, e, f and F shows the morphology of Ti5Cu samples before and after etching under optical microscope (Fig. 2E and F) and high magnification SEM (Fig. 2e and f). Obvious acicular α grains can be observed on the surface before etching (Fig. 2E), and Ti₂Cu precipitates were observed under high magnification SEM (Fig. 2e). A small amount of α grains could still be observed (Fig. 2F). Small pits appeared on the surface after etching (Fig. 2f). After surface treatment (etching), observing the microstructure of the samples (grinding and polishing treatment is required) will destroy the surface morphology. The existing technology cannot observe the microstructure in situ after etching, as shown in Fig. 2f. Fig. 2g and h shows the EDS analysis of Ti5Cu samples before and after etching. Result shows that the distribution of Cu was not affected by etching, and only a small amount of Cu-containing phase is preferentially dissolved.

Fig. 2I presents the XRD patterns of TC4 and Ti5Cu samples before and after etching. All the samples exhibited α -Ti as a single phase, and Ti₂Cu were detected in Ti5Cu and ETi5Cu groups. Fig. 2J shows the surface roughness of TC4 scaffolds and Ti5Cu scaffolds before and after surface treatment. The average three-dimensional roughness (S_a) of etched TC4 and Ti5Cu scaffolds was significantly lower than that unetched TC4 and Ti5Cu scaffolds respectively ($p < 0.05$). There was no significant difference between the S_a value of TC4 and Ti5Cu scaffolds.

3.2. Cells cultured on Ti alloy scaffolds

3.2.1. Cells proliferation and cytotoxicity

The effects of Ti alloy scaffolds on the proliferation of MC3T3-E1 cells are shown in Fig. 3. It was found that the OD values of all groups cultured with MC3T3-E1 cells increased gradually with the culture time. At 1 d, the absorbance of ETC4 and ETi5Cu groups were significantly higher than TC4 group ($p < 0.05$). At 3 d, 5 d and 7 d, the absorbance of ETC4 and Ti5Cu groups were significantly higher than TC4 group ($p < 0.05$), and the absorbance of ETi5Cu

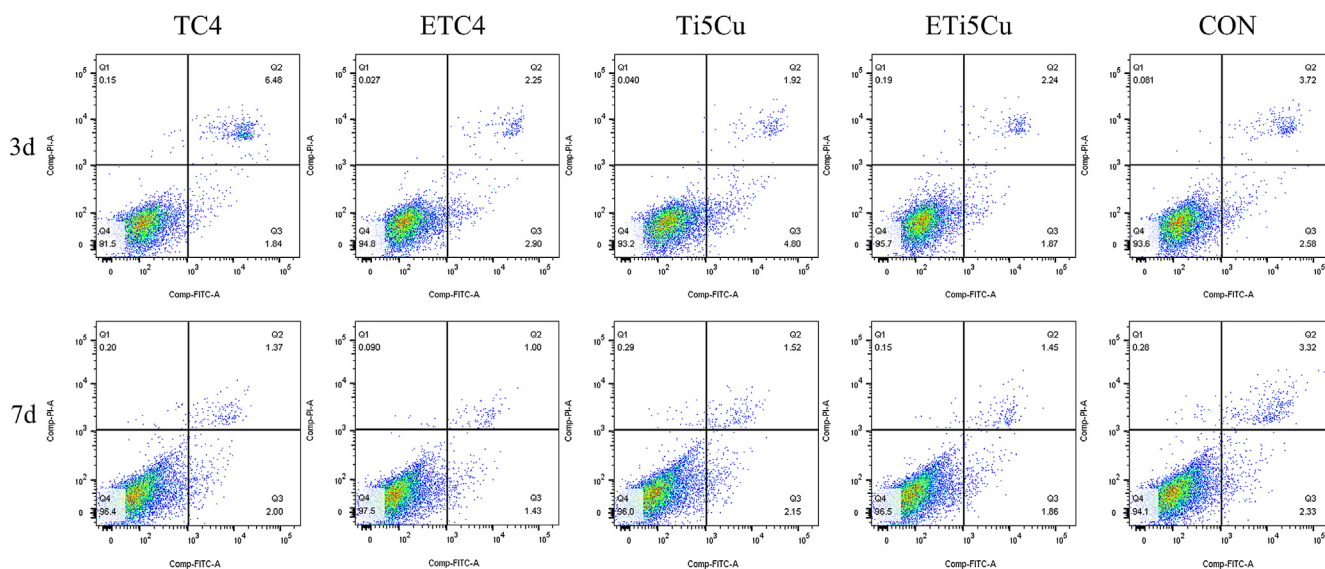


Fig. 4. Apoptosis of MC3T3-E1 cells cultured with Ti alloy scaffolds for 3d and 7d.

group was significantly higher than Ti5Cu group ($p < 0.05$). Moreover, at 5 d and 7 d, the absorbance of ETC4 group was significantly higher than Ti5Cu group ($p < 0.05$). The cell toxicity grade (CTG) was obtained according to the standard United States Pharmacopeia [45]. From 1 d to 7 d of incubation, all groups showed grade 0 to 1 (no toxicity).

3.2.2. Apoptosis of MC3T3-E1 cells

Apoptosis is normal physiological process of the cell death, and apoptosis rate can reflect the adaptation ability of cells to different surfaces. The lower left quadrant (Q4) represents living cells, the upper right quadrant (Q2) contains late apoptotic cells and necrotic cells, and the lower right quadrant (Q3) stands for early apoptotic cells. Fig. 4 shows the apoptosis of MC3T3-E1 cells incubated with untreated and treated Ti alloy scaffolds at different time points

were examined by flow cytometry. At 3 d, the early apoptosis rate of ETi5Cu group was 1.87%, which was significantly lower than that of Ti5Cu group 4.8%. At 7 d, the early apoptosis rate of ETC4 group was 1.43%, which was slightly lower than that of TC4 group 2 %, and the early apoptosis rate of ETi5Cu group was 1.86 %, which was lower than that of Ti5Cu group 2.15%.

3.2.3. ALP activity and Alizarin red staining

Fig. 5A shows ALP activity of MC3T3-E1 cells cultured with Ti alloy scaffolds for 7 d and 14 d. It was found that ALP content of all groups increased as osteogenic induction time prolonged. At the time point of 7 d and 14 d, ALP content of ETC4 group and ETi5Cu group were significantly higher than that of TC4 group and Ti5Cu group ($p < 0.05$), respectively. At 14 d, ALP content of Ti5Cu group and ETi5Cu group were significantly higher than that

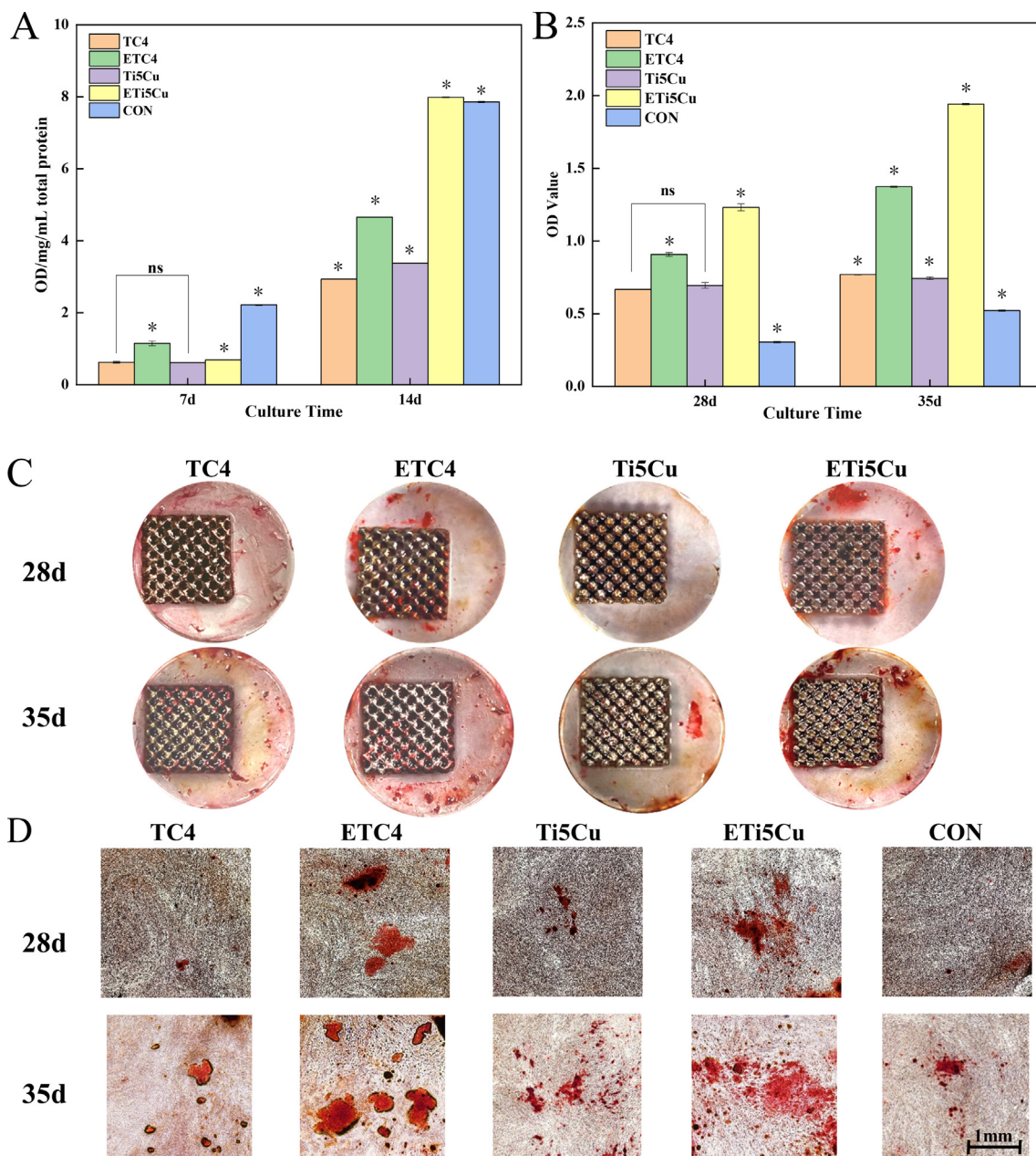


Fig. 5. (A) ALP activity of MC3T3-E1 cells cultured with Ti alloy scaffolds for 7 d and 14 d ($n = 3$, $* p < 0.05$). (B-D) Alizarin red staining of MC3T3-E1 cells cultured with Ti alloy scaffolds for 28 d and 35 d; (B) The quantified optical density of Alizarin red; (C) Photographs of Ti alloy scaffolds after Alizarin red staining; (D) $10 \times$ images under inverted phase contrast microscope.

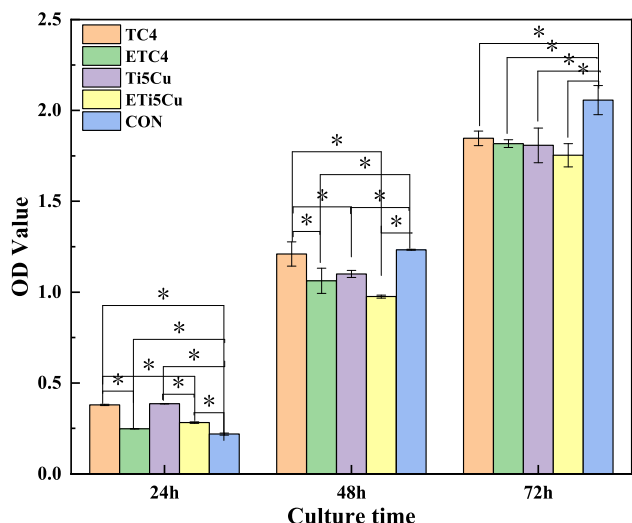


Fig. 6. Optical density of RAW 264.7 cells cultured on different Ti alloy scaffolds at different detection period (n = 5, * p < 0.05).

of TC4 group and ETC4 group (p < 0.05), respectively. In addition, ALP content of ETi5Cu group was the highest among the four experimental groups at 14 d. As shown in Fig. 5B, the quantified optical density of Alizarin red was significantly higher in ETC4 and ETi5Cu groups compared to the TC4 and Ti5Cu groups. Moreover, stronger Alizarin red staining was observed in the wells co-cultured with ETC4 and ETi5Cu scaffolds, and red granular precipitates were observed in the both groups under inverted phase contrast microscope (Nikon Corporation, Japan) (Fig. 5C and D).

3.2.4. Macrophages proliferation

Fig. 6 shows the optical densities of RAW 264.7 cells cultured on different Ti alloy scaffolds. The absorbance of all the experimental groups showed lower than the control group (p < 0.05). At 24 h, the absorbance of ETC4 and ETi5Cu group showed significantly lower than TC4 and Ti5Cu group (p < 0.05), respectively. At 48 h, the absorbance of TC4 group showed significantly higher than ETC4, Ti5Cu and ETi5Cu group (p < 0.05). At 72 h, there was no significant difference among all the experimental groups (p greater than 0.05).

3.2.5. Macrophages polarization

Fig. 7 shows the expression of M1 marker CD86 and M2 marker CD206 in RAW 264.7 cells cultured on different Ti alloy scaffolds for 24 h. It was observed that the expression of CD86 in ETi5Cu group was the lowest and in ETC4 group was the highest among all groups. The expression of CD206 in the ETC4 group was the lowest and in Ti5Cu group was the highest among all groups. In addition, the expression level of CD86 in ETi5Cu group

was lower, while the expression of CD206 in that was at a higher level.

3.3. Cell responses to metal powders

3.3.1. Cell proliferation and cytotoxicity test

Fig. 8 shows the optical densities of MC3T3-E1 cells cultured with different metal powders were measured by the CCK8 test. At 1 d, there was no significant difference among PTC4-0.5 mg/mL, PTC4-1 mg/mL and PTC4-3 mg/mL group, the absorbance of PTi5Cu-0.5 mg/mL group were significantly higher than PTi5Cu-1 mg/mL group (p < 0.05). At 3 d, 5 d and 7 d, the absorbance of PTC4 and PTi5Cu groups decreased significantly with the increase of powder concentration (p < 0.05).

3.3.2. Cell apoptosis assay

Fig. 9 shows the apoptosis of MC3T3-E1 cells cultured with metal powders at different time points were examined by flow cytometry. At 3 d, the early apoptosis rate of PTC4-0.5 mg/mL, PTC4-1 mg/mL and PTC4-3 mg/mL group were 1.62%, 4.65%, and 5.82%, the early apoptosis rate of PTi5Cu-0.5 mg/mL, PTi5Cu-1 mg/mL and PTi5Cu-3 mg/mL were 1.33%, 2.41%, and 6.42%. At 7 d, the early apoptosis rate of PTC4-0.5 mg/mL, PTC4-1 mg/mL and PTC4-3 mg/mL group were 1.78%, 2.91%, and 3.34%, the early apoptosis rate of PTi5Cu-0.5 mg/mL, PTi5Cu-1 mg/mL and PTi5Cu-3 mg/mL were 0.8%, 1.53%, and 5.35%. The early apoptosis rate of PTC4 and PTi5Cu groups increased significantly with the increase of powder concentration.

3.3.3. ALP activity and Alizarin red staining

Fig. 10A shows ALP activity of MC3T3-E1 cells cultured with metal powders for 7 d and 14 d. It was found that ALP content of all groups increased as osteogenic induction time prolonged. At 7 d and 14 d, ALP content of PTC4 and PTi5Cu groups decreased significantly with the increase of powder concentration. As shown in Fig. 10B, the quantified optical density of Alizarin red was significantly higher in the PTC4-0.5 mg/mL and PTi5Cu-0.5 mg/mL groups compared to the higher concentration groups. Moreover, stronger Alizarin red staining was observed in the wells co-cultured with lower concentration TC4 and Ti5Cu powders, and red granular precipitates were observed in these groups under inverted phase contrast microscope (Nikon Corporation, Japan) (Fig. 10C and D).

3.3.4. Macrophage proliferation

Fig. 11 shows the optical densities of RAW 264.7 cells cultured with metal powders at different time points. At 24 h, 48 h and 72 h, the absorbance of PTC4-3 mg/mL showed significantly lower than PTC4-1 mg/mL and PTC4-0.5 mg/mL groups (p < 0.05), the absorbance of PTi5Cu-3 mg/mL showed significantly lower than PTi5Cu-0.5 mg/mL and PTi5Cu-1 mg/mL groups.

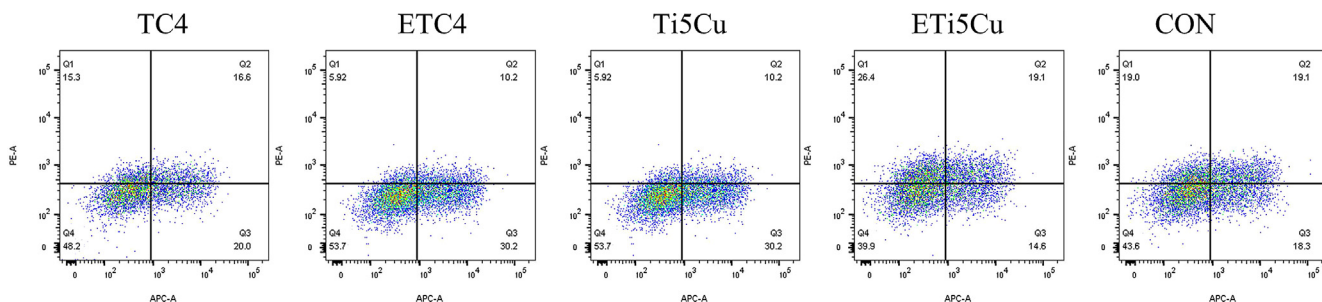


Fig. 7. Flow cytometry analysis of macrophage surface markers for 24 h (CD86 is detected by APC channel; CD206 is detected by PE channel).

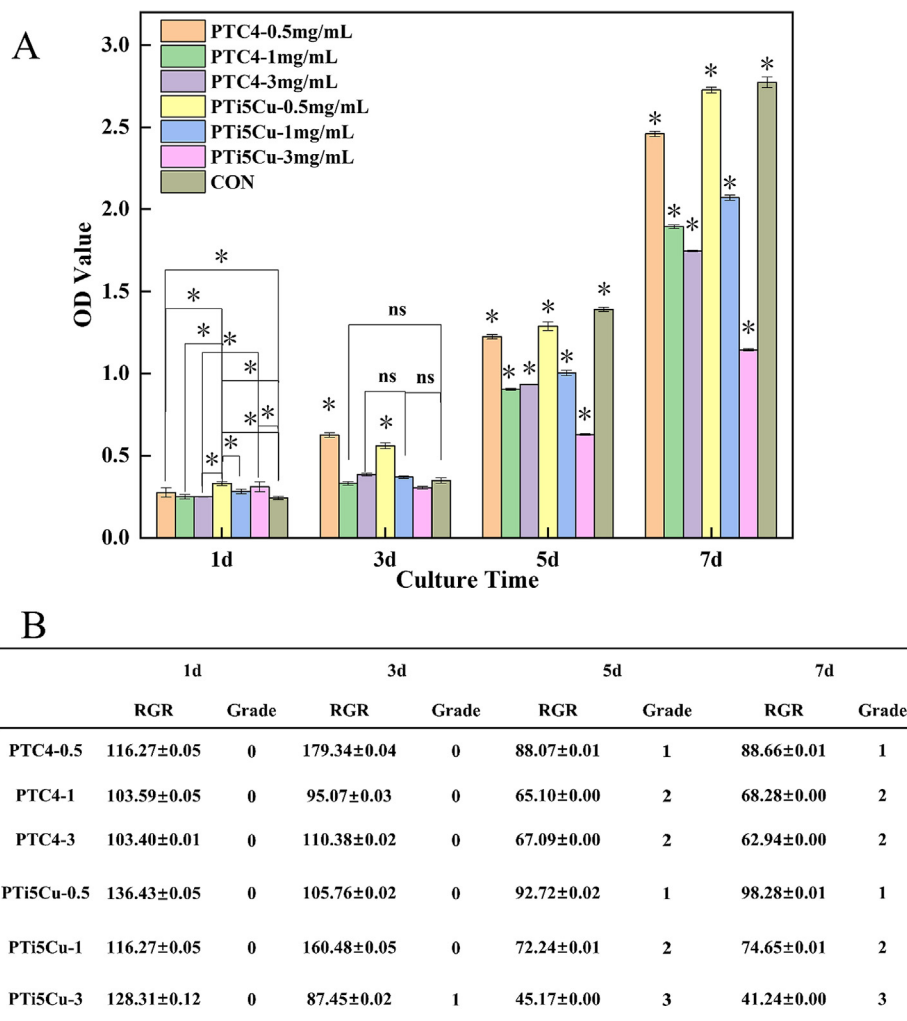


Fig. 8. (A) Optical density of MC3T3-E1 cells measured by CCK8 test and (B) relative growth rate (RGR) and cytotoxicity level at different detection period ($n = 5$, $* p < 0.05$).

3.3.5. Macrophage polarization

Fig. 12 shows the expression of M1 marker CD86 and M2 marker CD206 in RAW 264.7 cells cultured with metal powders for 24 h. It was observed that the expression of CD86 in all groups was at a higher level. The expression of CD206 in the PTC4-0.5 mg/mL group and PTC4-1 mg/mL group was at a higher level and in PTi5Cu-0.5 mg/mL group and PTi5Cu-1 mg/mL group was at a lower level. In addition, the expression level of CD86 in PTi5Cu-1 mg/mL group was higher, while the expression of CD206 in that was at a lower level.

4. Discussion

4.1. The scaffold structures

Manufacturing of the 3D patient-specific metallic scaffold with controlled architecture is possible by 3D printing technology. The presence of pores provide space for cell migration, connection, proliferation, and differentiation, thereby facilitating the growth of cells, blood vessels, as well as tissues, and enhancing the ability of bone integration. In this context, it is important to characterize the size and shape of the pores in order to study its effect on biological behavior. Too large or too small pores have adverse effects on cells [7]. Some studies showed that porous Ti structures with controlled pore size in the range of 500 μm -1500 μm can be ben-

eficial for faster integration of porous implant with host bone tissue [8]. In this study, all the porous samples had no adverse effects on the proliferation and differentiation of MC3T3-E1 cells and RAW 264.7 cells, indicating that the porous titanium alloy with a rhomboid porous structure and the size of 500 μm in the current work was suitable for cell growth.

In the 3D printing process, objects can be fabricated from elemental powders based on the computer aided design models [46]. Laser printing in a powder bed provides a possibility to fabricate objects of any shape in one production step. However, in the processing of 3D printing technology, the un-melted metal powders adhered on the Ti alloy scaffolds during the solidification process. As can be seen from Fig. 2, powders were trapped on the connection part and the inner surface of the scaffold. Hence, in the case of a cellular pore structure of a few hundred micrometers, removal of the un-melted powders can be done by chemical methods instead of the conventional post-processing such as machining or vibro-abrasive machining. In this study, the surface treatment based on hydrofluoric acid solution can be successfully used to remove the residual powders attached on Ti alloy scaffolds. Moreover, the distribution of Cu was not affected by etching, and only a small amount of Cu-containing phase is preferentially dissolved (Fig. 2g and h). Since the corrosion potentials of the Ti_2Cu and the matrix are different, a certain amount of galvanic corrosion will inevitably occur. A

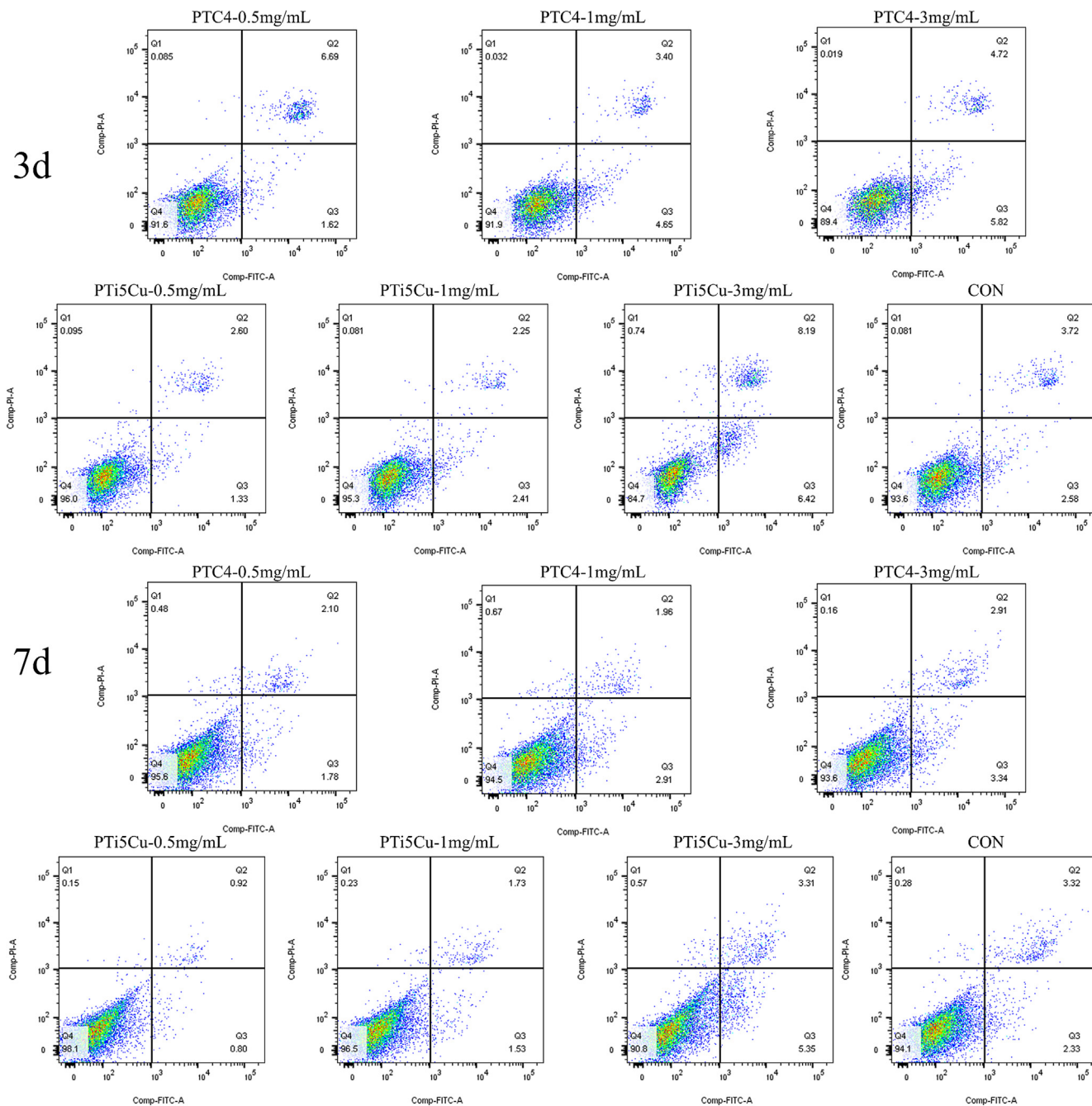


Fig. 9. Apoptosis of MC3T3-E1 cells cultured with metal powders for 3 d and 7 d.

similar phenomenon is also introduced in the document [47]. But, the galvanic corrosion of Cu-containing Ti alloy can be ignored because the passive film of Ti alloy has a good protective effect. Besides, the surface roughness of the scaffolds sample decreases after etching. This is because powders on the surface of the sample make the sample uneven and has large undulations, while the sample relatively smooth due to small pits appear on the sample surface after etching. Therefore, the surface treatment in this study has no significant effect on the microstructure of the sample, but only achieved the effect of removing powder and reducing the surface roughness of the sample.

4.2. In vitro cytocompatibility of MC3T3-E1 cells

One of the problems of biomaterials used is the surface contamination with residues or powders within the production process. These powders can accumulate in the tissue surrounding the implant, which can cause related cells such as osteoblasts, macrophages and osteoclasts to interact in various fashions, resulting in implant failure. Studies found that the powder produced by implants can lead to osteolysis of bone tissue [48-50]. In order to demonstrate the effect of surface residual powders on the biological properties of scaffold samples, this study further explored the role of different concentrations of metal powders on MC3T3-E1

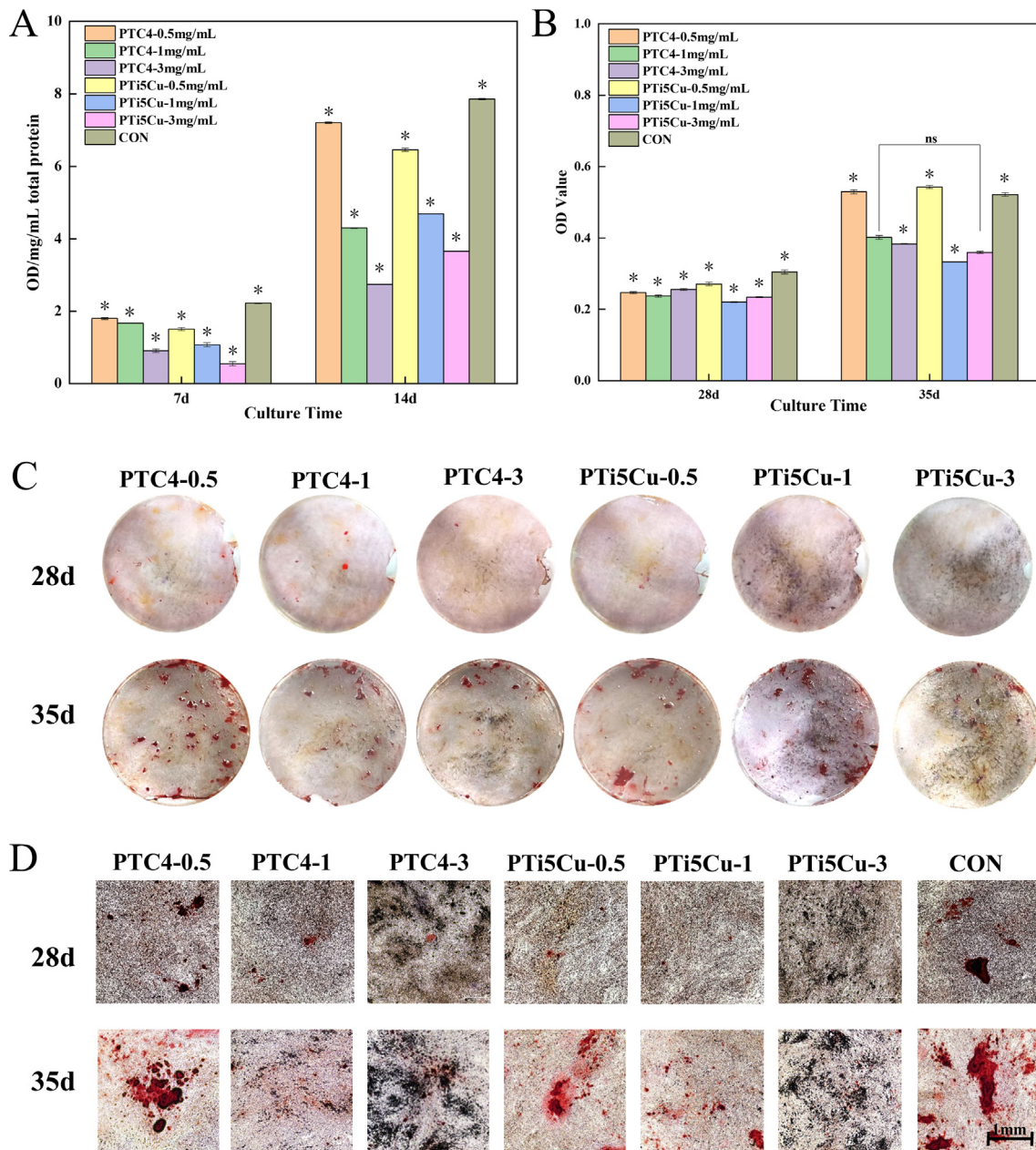


Fig. 10. (A) ALP activity of MC3T3-E1 cells cultured with Ti alloy powders for 7 d and 14 d (n = 3, * p < 0.05). (B-D) Alizarin red staining of MC3T3-E1 cells cultured with Ti alloy scaffolds for 28 d and 35 d: (B) The quantified optical density of Alizarin red; (C) Photographs of Ti alloy scaffolds after Alizarin red staining; (D) 10 × images under inverted phase contrast microscope.

cells and RAW 264.7 cells. Results showed that the absorbance of etched samples (including ETC4 and ETi5Cu scaffolds) were significantly higher than unetched samples (including TC4 and Ti5Cu scaffolds). Similar results have also been shown in the increased roughness of the samples. However, the surface roughness of the sample decreases after etching in this study. Moreover, high concentrations of metal powders significantly inhibited proliferation of MC3T3-E1 cells, showing cytotoxicity, and the higher the concentration could increase the toxicity grade (Fig. 8). Therefore, these results indicated that the etched sample can promote cell proliferation mainly due to the removal of surface powders. The level of apoptosis rate reflects the state of cells on the surface of the material. In this study, the early apoptosis rate of PTC4 and PTi5Cu groups increased significantly with the increase of powder concentration, which consistent with the phenomenon that the

apoptosis rate in etched groups (including ETC4 group and ETi5Cu group) showed lower than that in unetched groups. Moreover, the apoptosis rate of the 3 mg/mL powder group was always higher than that of the scaffolds sample group. This is because, on the one hand, the release of solid alloy ions was less than the release of metal powder [51], thus promoting the apoptosis of osteoblasts. On the other hand, the existence of powder particles induces cell apoptosis.

ALP as one of the early markers of osteogenesis, can directly reflect early stages of osteoblast differentiation and maturation [52]. In this study, the ALP activity of the samples with removal of the un-melted powders from their surface showed higher than that of the untreated samples, which is consistent with the results of the high and low concentration powder group (Fig. 10). As shown in Fig. 10A, ALP activity of the cells treated with 1 mg/mL

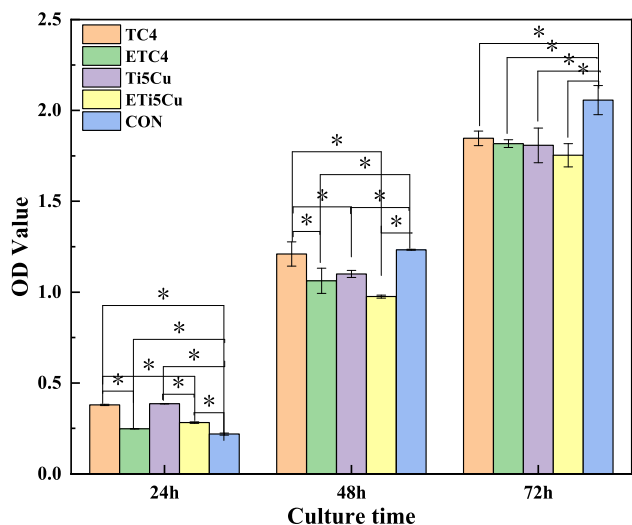


Fig. 11. Optical density of RAW264.7 cells cultured with metal powders at different detection period. (n = 5, * p < 0.05).

and 3 mg/mL of metal powders in the experimental group was significantly lower than that of the control group, so the metal powders inhibited early osteogenic differentiation of MC3T3-E1 cells. This may be because when co-culture with metal powders, MC3T3-E1 cells were directly exposed to metal powders, resulting in reducing the expression of factors related to osteoblast differentiation and weakened mineralization ability [53,54]. In addition, ALP content of PTC4 and PTi5Cu groups decreased significantly with the increase of powder concentration, indicating the inhibitory effect of high-concentration powder on osteogenesis was more significant. Calcified nodules are the latter expression of osteogenic phenotype of osteoblasts in vitro culture. Stronger Alizarin red staining was observed in the etched groups than unetched groups. Moreover, all powder groups had fewer numbers of nodules and lighter Alizarin red staining, which indicated that the powder on the surface of the sample can significantly inhibit the osteogenic mineralization ability of the MC3T3-E1 cells. Moreover, material characterization showed etching had no significant effect on the microstructure of the sample. Therefore, the etched samples showed the better cytocompatibility mainly due to the removal of surface powders.

In addition, it was reported that Cu could promote proliferation and differentiation of osteoblasts, collagen deposition and calcification of bone [55]. Other studies have demonstrated that Cu ions has inhibitory effects on the proliferation of osteoblasts [56]. According to the results of the apoptosis experiment in this study, an appropriate amount of Cu does not improve the apoptosis of cells, this result is in line with the finding in the relevant studies [57-59]. Furthermore, ALP activity of MC3T3-E1 cells in the

Cu-bearing scaffolds groups was higher than that of Cu-free scaffolds groups, which indicated that the addition of Cu could promote early osteogenic differentiation of MC3T3-E1 cells and the osteogenic performance could be further improved after the removal of alloy powder. Based on the above results, we found that ETi5Cu group with stable and higher proliferation rate, lowest apoptosis rate and the best early osteogenic ability was more conducive to cell proliferation.

4.3. Biological behaviors of RAW 264.7 cells

The alloy composition, structure and surface morphology of the scaffold could affect the macrophage behaviors. RAW 264.7 cells as the functional macrophage line are commonly used to study the anti-inflammatory properties of drugs or biomaterials. Macrophages swallow damaged tissue fragments and release factors that promote repair, thus initiating the process of tissue repair and regeneration [60]. Therefore, macrophages are the key cells for successful bone formation and remodeling. It was reported that reducing the number of macrophages would inhibit the production of growth factors in the repair process, which adversely affect tissue healing [61]. However, too many macrophages may cause a strong immune response, which can easily lead to implant failure. In the current work, the results of CCK8 assay showed that ETC4 group and ETi5Cu group exhibited a slight inhibitory effect on cell proliferation and viability of macrophages (Fig. 6), which was conducive to subsequent repair and regeneration. In addition, lower concentrations of powder have a tendency to promote macrophage proliferation (Fig. 11), which may be because the powder stimulates the phagocytic function of macrophages, thus leading to the increase of cell viability [62]. This explains the phenomenon that the proliferation of macrophages in surface treated group (including ETC4 group and ETi5Cu group) showed higher than that in untreated group.

The osseointegration process around the implant is affected by the polarization of macrophages [63]. Generally, M1 type macrophages are responsible for inducing and regulating the inflammatory environment, promoting the generation and activation of osteoclasts, and M2 type macrophages are responsible for anabolism, which is beneficial to bone formation and mineralization [64]. Studies have shown that the shedding of titanium particles on the surface of the implant promotes the polarization of macrophages to M1 type [31,65]. This is consistent with the results of the influence of titanium alloy powder on the polarization of macrophages in this study (Fig. 12). As shown in Fig. 12, the high concentration of powders could induce macrophages to polarization toward M1 type. Moreover, it is widely accepted that the residual powder is one of the main causes of aseptic loosening [66]. In the present work, regardless of high concentration or low concentration, residual powders can affect the proliferation and polarization of macrophages. Moreover, Cu has been shown to

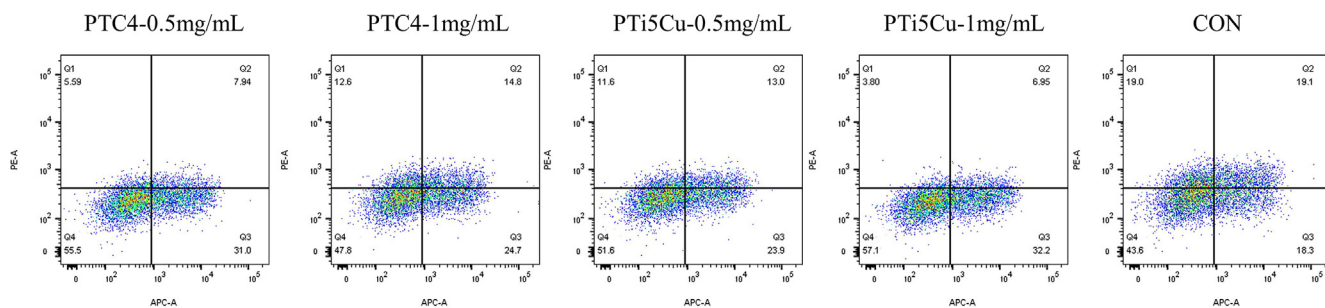


Fig. 12. Flow cytometry analysis of macrophage surface markers for 24 h (CD86 is detected by APC channel; CD206 is detected by PE channel).

decrease inflammation by inhibiting the proliferation of macrophages, and also by increasing macrophage production of anti-inflammatory factors [42,67]. In this study, ETi5Cu group showed promoting the conversion of macrophages to the anti-inflammatory M2 phenotype. This is on the one hand due to the removal of surface metal powder particles and on the other hand attributed to the addition of Cu. Therefore, ETi5Cu possesses the potential to reduce the inflammatory response by inhibiting the proliferation of macrophages and promoting the polarization of macrophages to M2 type.

5. Conclusions

In this study, the effects of the unfused metal powders on the biological properties of 3D printed Ti alloy scaffolds were assessed by co-culture with MC3T3-E1 cells and RAW 264.7 cells. The results showed that the removal of residual powders on the scaffolds is a very important for the biological performance improvement. The following conclusions can be drawn:

- (1) Surface treatment enhanced the proliferation and differentiation of MC3T3-E1 cells and inhibit cell apoptosis compared with the untreated scaffolds.
- (2) All scaffold samples showed no toxicity to MC3T3-E1 cells, in particular, ETi5Cu scaffolds showed stable and higher proliferation rate, lowest apoptosis rate and the best osteogenic ability, which was more conducive to the growth of osteoblasts.
- (3) ETi5Cu possessed the potential to reduce the inflammatory response by promoting the polarization of macrophages to M2 type.
- (4) The powders on the surface of 3D printed Ti alloy scaffolds inhibited the proliferation and early osteogenic differentiation of MC3T3-E1 cells, as well as promoted apoptosis.

CRedit authorship contribution statement

Zhe Yi: Methodology, Writing – review & editing. **Ying Liu:** Methodology, Writing – review & editing, Writing – original draft. **Yidan Ma:** Methodology, Writing – review & editing. **Zhaogang Liu:** Writing – original draft. **Hui Sun:** Investigation, Formal analysis. **Xing Zhou:** Investigation, Formal analysis. **Rui Kang:** Investigation, Formal analysis. **V.A.M. Cristino:** Investigation, Formal analysis. **Qiang Wang:** Supervision, Funding acquisition.

Declaration of Competing Interest

The authors declare that they have no known competing financial interests or personal relationships that could have appeared to influence the work reported in this paper.

Acknowledgments

This work was supported by the Shenyang Science and Technology Program (No. 19-112-4-029), the Natural Science Foundation Project of Liaoning Province (2020-MS-150, 2018225059) and Shenyang Science and Technology Funded Project (RC190290).

References

- [1] S.K. Nishimoto, M. Nishimoto, S.W. Park, K.M. Lee, H.S. Kim, J.T. Koh, J.L. Ong, Y. Liu, Y. Yang, The Effect of Titanium Surface Roughening on Protein Absorption, Cell Attachment, and Cell Spreading, *The International Journal of Oral & Maxillofacial Implants* 23 (2008) 675–680.
- [2] Y. Tian, S. Ding, H. Peng, S. Lu, G. Wang, L.u. Xia, P. Wang, Osteoblast growth behavior on porous-structure titanium surface, *Appl. Surf. Sci.* 261 (2012) 25–30.
- [3] Y. Xiong, W. Wang, R. Gao, H. Zhang, L. Dong, J. Qin, B. Wang, W. Jia, X. Li, Fatigue behavior and osseointegration of porous Ti-6Al-4V scaffolds with dense core for dental application, *Mater. Des.* 195 (2020) 108994.
- [4] L. Li, Y. Chen, Y. Lu, S. Qin, G. Huang, T. Huang, J. Lin, Effect of heat treatment on the corrosion resistance of selective laser melted Ti6Al4V3Cu alloy, *J. Mater. Res. Technol.* 12 (2021) 904–915.
- [5] A. Cheng, A. Humayun, D.J. Cohen, B.D. Boyan, Z. Schwartz, Additively manufactured 3D porous Ti-6Al-4V constructs mimic trabecular bone structure and regulate osteoblast proliferation, differentiation and local factor production in a porosity and surface roughness dependent manner, *Biofabrication* 6 (4) (2014) 045007, <https://doi.org/10.1088/1758-5082/6/4/045007>.
- [6] A. Kumar, K.C. Nune, L.E. Murr, R.D.K. Misra, Biocompatibility and mechanical behaviour of three-dimensional scaffolds for biomedical devices: process-structure-property paradigm, *Int. Mater. Rev.* 61 (1) (2016) 20–45.
- [7] C.E. Wen, M. Mabuchi, Y. Yamada, K. Shimojima, Y. Chino, T. Asahina, Processing of biocompatible porous Ti and Mg, *Scr. Mater.* 45 (10) (2001) 1147–1153.
- [8] W. Xue, B.V. Krishna, A. Bandyopadhyay, S. Bose, Processing and biocompatibility evaluation of laser processed porous titanium, *Acta Biomater.* 3 (6) (2007) 1007–1018.
- [9] V. Karageorgiou, D. Kaplan, Porosity of 3D biomaterial scaffolds and osteogenesis, *Biomaterials* 26 (27) (2005) 5474–5491.
- [10] Q. Ran, W. Yang, Y. Hu, X. Shen, Y. Yu, Y. Xiang, K. Cai, Osteogenesis of 3D printed porous Ti6Al4V implants with different pore sizes, *J Mech Behav Biomed Mater* 84 (2018) 1–11.
- [11] R.A. Perez, G. Mestres, Role of pore size and morphology in musculo-skeletal tissue regeneration, *Mater Sci Eng C Mater Biol Appl* 61 (2016) 922–939.
- [12] H. Wang, K. Su, L. Su, P. Liang, P. Ji, C. Wang, The effect of 3D-printed Ti6Al4V scaffolds with various macropore structures on osteointegration and osteogenesis: A biomechanical evaluation, *J Mech Behav Biomed Mater* 88 (2018) 488–496.
- [13] T.i. Yu, H. Gao, T. Liu, Y. Huang, C. Wang, Effects of immediately static loading on osteogenesis and osteogenesis around 3D-printed porous implant: A histological and biomechanical study, *Mater Sci Eng C Mater Biol Appl* 108 (2020) 110406, <https://doi.org/10.1016/j.msec.2019.110406>.
- [14] C. Han, Y. Li, Q. Wang, S. Wen, Q. Wei, C. Yan, L. Hao, J. Liu, Y. Shi, Continuous functionally graded porous titanium scaffolds manufactured by selective laser melting for bone implants, *J Mech Behav Biomed Mater* 80 (2018) 119–127.
- [15] A. Civantos, C. Domínguez, R.J. Pino, G. Setti, J.J. Pavón, E. Martínez-Campos, F.J. García García, J.A. Rodríguez, J.P. Allain, Y. Torres, Designing bioactive porous titanium interfaces to balance mechanical properties and in vitro cells behavior towards increased osseointegration, *Surf. Coat. Technol.* 368 (2019) 162–174.
- [16] G. Yu, Z. Li, S. Li, Q. Zhang, Y. Hua, H. Liu, X. Zhao, D.T. Dhaidhai, W. Li, X. Wang, The select of internal architecture for porous Ti alloy scaffold: A compromise between mechanical properties and permeability, *Mater. Des.* 192 (2020) 108754.
- [17] M. Croes, S. Bakhshandeh, I.A.J. van Hengel, K. Lietaert, K.P.M. van Kessel, B. Pouran, B.C.H. van der Wal, H.C. Vogely, W. Van Hecke, A.C. Fluit, C.H.E. Boel, J. Alblas, A.A. Zadpoor, H. Weinans, S. Amin Yavari, Antibacterial and immunogenic behavior of silver coatings on additively manufactured porous titanium, *Acta Biomater* 81 (2018) 315–327.
- [18] Y. Wang, H. Cui, J. Zhou, F. Li, J. Wang, M. Chen, Q. Liu, Cytotoxicity, DNA damage, and apoptosis induced by titanium dioxide nanoparticles in human non-small cell lung cancer A549 cells, *Environ Sci Pollut Res Int* 22 (7) (2015) 5519–5530.
- [19] L. Roncati, A.M. Gatti, T. Pusioli, G. Barbolini, A. Maiorana, S. Montanari, ESEM Detection of Foreign Metallic Particles inside Ameloblastomatous Cells, *Ultrastruct Pathol* 39 (5) (2015) 329–335.
- [20] T. Fretwurst, G. Buzanich, S. Nahles, J.P. Woelber, H. Riesemeier, K. Nelson, Metal elements in tissue with dental peri-implantitis: a pilot study, *Clin Oral Implants Res* 27 (9) (2016) 1178–1186.
- [21] D.G. Olmedo, G. Nalli, S. Verdu, M.L. Paparella, R.L. Cabrini, Exfoliative cytology and titanium dental implants: a pilot study, *J Periodontol* 84 (1) (2013) 78–83.
- [22] J.H. Dumbleton, M.T. Manley, Metal-on-Metal total hip replacement: what does the literature say?, *J Arthroplasty* 20 (2) (2005) 174–188.
- [23] N. Wang, S. Maskomani, G.K. Meenashisundaram, J.Y.H. Fuh, S.T. Dheen, S.K. Anantharajan, A study of Titanium and Magnesium particle-induced oxidative stress and toxicity to human osteoblasts, *Mater Sci Eng C Mater Biol Appl* 117 (2020) 111285.
- [24] B.V. Hooreweder, K. Lietaert, B. Neirincx, N. Lippiatt, M. Wevers, CoCr F75 scaffolds produced by additive manufacturing: Influence of chemical etching on powder removal and mechanical performance, *J Mech Behav Biomed Mater* 70 (2017) 60–67.
- [25] M.G. Choi, H.S. Koh, D. Kluess, D. O'Connor, A. Mathur, G.A. Truskey, J. Rubin, D. X.F. Zhou, K.-L. P. Sung, Effects of titanium particle size on osteoblast functions in vitro and in vivo, *PNAS* 102 (12) (2005) 4578–4583.
- [26] Y. Wang, H. Liu, J. Wu, Y. Liao, D. Lu, F. Dong, H. Li, Z. Zhang, Y. Lian, 5-Aza-2-deoxycytidine inhibits osteolysis induced by titanium particles by regulating RANKL/OPG ratio, *Biochem Biophys Res Commun* 529 (3) (2020) 629–634.
- [27] Z. Zhang, X. Fu, L. Xu, X. Hu, F. Deng, Z. Yang, L. Jiang, T. Fu, P. Zhou, J. Song, P. Ji, J. Huang, X. Wu, Nanosized Alumina Particle and Proteasome Inhibitor Bortezomib Prevented inflammation and Osteolysis Induced by Titanium Particle via Autophagy and NF- κ B Signaling, *Sci. Rep.* 10 (1) (2020), <https://doi.org/10.1038/s41598-020-62254-x>.

- [28] W. Xu, C. Hou, Y. Mao, L. Yang, M. Tamaddon, J. Zhang, X. Qu, C. Liu, B.o. Su, X. Lu, Characteristics of novel Ti-10Mo-xCu alloy by powder metallurgy for potential biomedical implant applications, *Bioact Mater* 5 (3) (2020) 659–666.
- [29] G.J. Atkins, D.R. Haynes, D.W. Howie, D.M. Findlay, Role of polyethylene particles in peri-prosthetic osteolysis: A review, *World J Orthop* 2 (10) (2011) 93–101.
- [30] J. Gallo, S.B. Goodman, Y.T. Konttinen, M. Raska, Particle disease: biologic mechanisms of periprosthetic osteolysis in total hip arthroplasty, *Innate Immun* 19 (2) (2013) 213–224.
- [31] X. Wang, Y.u. Li, Y. Feng, H. Cheng, D. Li, Macrophage polarization in aseptic bone resorption around dental implants induced by Ti particles in a murine model, *J Periodontol Res* 54 (4) (2019) 329–338.
- [32] N.J. Horwood, Macrophage Polarization and Bone Formation: A review, *Clin Rev Allergy Immunol* 51 (1) (2016) 79–86.
- [33] P.J. Murray, J.E. Allen, S.K. Biswas, E.A. Fisher, D.W. Gilroy, S. Goerdt, S. Gordon, J.A. Hamilton, L.B. Ivashkiv, T. Lawrence, M. Locati, A. Mantovani, F.O. Martinez, J.L. Mege, D.M. Mosser, G. Natoli, J.P. Saeji, J.L. Schultze, K.A. Shirey, A. Sica, J. Suttles, I. Udalova, J.A. van Ginderachter, S.N. Vogel, T.A. Wynn, Macrophage activation and polarization: nomenclature and experimental guidelines, *Immunity* 41 (1) (2014) 14–20.
- [34] M. Eger, S. Hiram-Bab, T. Liron, N. Sterer, Y. Carmi, D. Kohavi, Y. Gabet, Mechanism and Prevention of Titanium Particle-Induced Inflammation and Osteolysis, *Front Immunol* 9 (2018) 2963.
- [35] A. Shapouri-Moghaddam, S. Mohammadian, H. Vazini, M. Taghadosi, S.-A. Esmaili, F. Mardani, B. Seifi, A. Mohammadi, J.T. Afshari, A. Sahebkar, Macrophage plasticity, polarization, and function in health and disease, *J Cell Physiol* 233 (9) (2018) 6425–6440.
- [36] M. Bost, S. Houdart, M. Oberli, E. Kalonji, J.-F. Huneau, I. Margaritis, Dietary copper and human health: Current evidence and unresolved issues, *J Trace Elem Med Biol* 35 (2016) 107–115.
- [37] T. Xi, M.B. Shahzad, D. Xu, Z. Sun, J. Zhao, C. Yang, M. Qi, K.e. Yang, Effect of copper addition on mechanical properties, corrosion resistance and antibacterial property of 316L stainless steel, *Mater Sci Eng C Mater Biol Appl* 71 (2017) 1079–1085.
- [38] E. Zhang, J. Ren, S. Li, L. Yang, G. Qin, Optimization of mechanical properties, biocorrosion properties and antibacterial properties of as-cast Ti-Cu alloys, *Biomed Mater* 11 (6) (2016) 065001, <https://doi.org/10.1088/1748-6041/11/6/065001>.
- [39] D. Zhang, Q.i. Han, K. Yu, X. Lu, Y. Liu, Z.e. Lu, Q. Wang, Antibacterial activities against *Porphyromonas gingivalis* and biological characteristics of copper-bearing PEO coatings on magnesium, *J Mater Sci Technol* 61 (2021) 33–45.
- [40] F. Lüthen, C. Bergemann, U. Bulnheim, C. Prinz, H.G. Neumann, A. Podbielski, R. Bader, J. Rychly, A Dual Role of Copper on the Surface of Bone Implants, *Mater. Sci. Forum* 638–642 (2010) 600–605.
- [41] S. Itoh, H.W. Kim, O. Nakagawa, K. Ozumi, S.M. Lessner, H. Aoki, K. Akram, R.D. McKinney, M. Ushio-Fukai, T. Fukai, Novel role of antioxidant-1 (Atox1) as a copper-dependent transcription factor involved in cell proliferation, *J Biol Chem* 283 (14) (2008) 9157–9167.
- [42] R. Lin, C. Deng, X. Li, Y. Liu, M. Zhang, C. Qin, Q. Yao, L. Wang, C. Wu, Copper-incorporated bioactive glass-ceramics inducing anti-inflammatory phenotype and regeneration of cartilage/bone interface, *Theranostics* 9 (21) (2019) 6300–6313.
- [43] W. Zhang, S. Zhang, H. Liu, L. Ren, Q. Wang, Y. Zhang, Effects of surface roughening on antibacterial and osteogenic properties of Ti-Cu alloys with different Cu contents, *J Mater Sci Technol* 88 (2021) 158–167.
- [44] W. Zong, S. Zhang, C. Zhang, L. Ren, Q. Wang, Design and characterization of selective laser-melted Ti6Al4V-5Cu alloy for dental implants, *Mater. Corros.* 71 (10) (2020) 1697–1710.
- [45] S. Jin, Y. Zhang, Q. Wang, D. Zhang, S. Zhang, Influence of TiN coating on the biocompatibility of medical NiTi alloy, *Colloids Surf., B* 101 (2013) 343–349.
- [46] O.L.A. Harrysson, D.J. Marcellin-Little, T.J. Horn, Applications of Metal Additive Manufacturing in Veterinary Orthopedic Surgery, *Jom* 67 (3) (2015) 647–654.
- [47] J. Wang, S. Zhang, Z. Sun, H. Wang, L. Ren, K.e. Yang, Optimization of mechanical property, antibacterial property and corrosion resistance of Ti-Cu alloy for dental implant, *J Mater Sci Technol* 35 (10) (2019) 2336–2344.
- [48] E. Sukur, Y.E. Akman, Y. Ozturkmen, F. Kucukdurmaz, Particle Disease: A Current Review of the Biological Mechanisms in Periprosthetic Osteolysis After Hip Arthroplasty, *Open Orthop J* 10 (2016) 241–251.
- [49] J. Bonini, K. Calaluca, M.J. Morra, Cleanliness and microstructural issues related to additive layer manufactured porous surface structured titanium medical and dental implants, in: *Proceedings of the 13th World Conference on Titanium*, 2016, pp. 1753–1759.
- [50] L.K. Longhofer, A. Chong, N.M. Strong, P.H. Wooley, S.Y. Yang, Specific material effects of wear-particle-induced inflammation and osteolysis at the bone-implant interface: A rat model, *J Orthop Translat* 8 (2017) 5–11.
- [51] R. Dong, W. Zhu, C. Zhao, Y. Zhang, F. Ren, Microstructure, Mechanical Properties, and Sliding Wear Behavior of Spark Plasma Sintered Ti-Cu Alloys, *Metallurgical and Materials Transactions A* 49 (12) (2018) 6147–6160.
- [52] X. Luo, J. Chen, W.-X. Song, N.i. Tang, J. Luo, Z.-L. Deng, K.A. Sharff, G. He, Y. Bi, B.-C. He, E. Bennett, J. Huang, Q. Kang, W. Jiang, Y. Su, G.-H. Zhu, H. Yin, Y. He, Y. i. Wang, J.S. Souris, L. Chen, G.-W. Zuo, A.G. Montag, R.R. Reid, R.C. Haydon, H. H. Luu, T.-C. He, Osteogenic BMPs promote tumor growth of human osteosarcomas that harbor differentiation defects, *Lab Invest* 88 (12) (2008) 1264–1277.
- [53] Y. Gu, Z. Wang, J. Shi, L. Wang, Z. Hou, X. Guo, Y. Tao, X. Wu, W. Zhou, Y. Liu, W. Zhang, Y. Xu, H. Yang, F. Xue, D. Geng, Titanium particle-induced osteogenic inhibition and bone destruction are mediated by the GSK-3beta/beta-catenin signal pathway, *Cell Death Dis* 8 (6) (2017) e2878.
- [54] J.-S. Nam, A.R. Sharma, S. Jagga, D.-H. Lee, G. Sharma, L.T. Nguyen, Y.H. Lee, J.-D. Chang, C. Chakraborty, S.-S. Lee, Suppression of osteogenic activity by regulation of WNT and BMP signaling during titanium particle induced osteolysis, *J Biomed Mater Res A* 105 (3) (2017) 912–926.
- [55] I. Burghardt, F. Lüthen, C. Prinz, B. Kreikemeyer, C. Zietz, H.-G. Neumann, J. Rychly, A dual function of copper in designing regenerative implants, *Biomaterials* 44 (2015) 36–44.
- [56] S. Li, M. Wang, X. Chen, S.-F. Li, J. Li-Ling, H.-Q. Xie, Inhibition of osteogenic differentiation of mesenchymal stem cells by copper supplementation, *Cell Prolif.* 47 (1) (2014) 81–90.
- [57] E. Zhang, L. Zheng, J. Liu, B. Bai, C. Liu, Influence of Cu content on the cell biocompatibility of Ti-Cu sintered alloys, *Mater Sci Eng C Mater Biol Appl* 46 (2015) 148–157.
- [58] L. Zhang, E.-M. Haddouti, K. Welle, C. Burger, D.C. Wirtz, F.A. Schildberg, K. Kabir, The Effects of Biomaterial Implant Wear Debris on Osteoblasts, *Front. Cell Dev. Biol.* 8 (352) (2020).
- [59] R. Liu, Z. Ma, S. Kunle Kolawole, L. Zeng, Y. Zhao, L. Ren, K. Yang, In vitro study on cytocompatibility and osteogenesis ability of Ti-Cu alloy, *J Mater Sci Mater Med* 30 (7) (2019) 75.
- [60] W. Zhang, X. Shen, L. Xie, M. Chu, Y. Ma, MicroRNA-181b regulates endotoxin tolerance by targeting IL-6 in macrophage RAW264.7 cells, *J Inflamm (Lond)* 12 (2015) 1–9.
- [61] R. Mirza, L.A. DiPietro, T.J. Koh, Selective and specific macrophage ablation is detrimental to wound healing in mice, *Am J Pathol* 175 (6) (2009) 2454–2462.
- [62] P.-A. Mouthuy, S.J. Snelling, S.G. Dakin, L. Milković, A. Čipak, A.J. Gašparović, N. Ž. Carr, Biocompatibility of implantable materials: an oxidative stress viewpoint, *Biomaterials* 109 (2016) 55–68.
- [63] Z. Liu, Y. Liu, S. Liu, D. Wang, J. Jin, L. Sun, Q. Wang, Z. Yi, The effects of TiO₂ nanotubes on the biocompatibility of 3D printed Cu-bearing TC4 alloy, *Mater. Des.* 207 (2021) 109831.
- [64] R.J. Miron, D.D. Bosshardt, OsteoMacs: Key players around bone biomaterials, *Biomaterials* 82 (2016) 1–19.
- [65] J.C. Tang, J.P. Luo, Y.J. Huang, J.F. Sun, Z.Y. Zhu, J.Y. Xu, M.S. Dargusch, M. Yan, Immunological response triggered by metallic 3D printing powders, *Addit. Manuf.* 35 (2020) 101392.
- [66] D. Olmedo, M.M. Fernández, M.B. Guglielmotti, R.L. Cabrini, Macrophages related to dental implant failure, *Implant Dent* 12 (1) (2003) 75–80.
- [67] X. Xu, Y. Lu, S. Li, S. Guo, M. He, K. Luo, J. Lin, Copper-modified Ti6Al4V alloy fabricated by selective laser melting with pro-angiogenic and anti-inflammatory properties for potential guided bone regeneration applications, *Mater Sci Eng C Mater Biol Appl* 90 (2018) 198–210.